EMISSIONS OF A WET PREMIXED FLAME OF NATURAL GAS AND A MIXTURE WITH HYDROGEN AT HIGH PRESSURE

P. Stathopoulos*, P. Kuhn, J. Wendler
T. Tanneberger, S. Terhaar, C. O. Paschereit
Chair of Fluid Dynamics
— Hermann-Föttinger-Institut —
Technische Universität Berlin
Müller-Breslau-Str 8, 10623 Berlin, Germany

C. Schmalhofer, P. Griebel, M. Aigner

German Aerospace Center (DLR),
Institute of Combustion Technology,
Pfaffenwaldring 38-40, 70569 Stuttgart, Germany

It is generally accepted that combustion of hydrogen and natural gas mixtures will become more prevalent in the near future, to allow for a further penetration of renewables in the European power generation system. The current work aims at the demonstration of the advantages of steam dilution, when highly reactive combustible mixtures are used in a swirl-stabilized combustor. To this end, high-pressure experiments have been conducted with a generic swirl-stabilized combustor featuring axial air injection to increase flashback safety. The experiments have been conducted with two fuel mixtures, at various pressure levels up to 9 bar and at four levels of steam dilution up to 25% steam-to-air mass flow ratio. Natural gas has been used as a reference fuel, whereas a mixture of natural gas and hydrogen (10% hydrogen by mass) represented an upper limit of hydrogen concentration in a natural gas network with hydrogen enrichment. The results of the emissions measurements are presented along with a reactor network model. The latter is applied as a means to qualitatively understand the chemical processes responsible for the observed emissions and their trends with increasing pressure and steam injection.

Nomenclature

LBO Lean blowout
PFR Plug flow reactor
PFZ Post flame zone
PSR Perfectly stirred reactor
p Absolute pressure
α Scaling exponent for emissions
ϕ Equivalence ratio
Ω Steam-to-air mass ratio

INTRODUCTION AND MOTIVATION

Combustion of hydrogen and hydrogen-enriched natural gas is steadily gaining attention in the power generation market. In an electric power system with high penetration of renewables, the production of hydrogen and its injection into the natural gas network offers a great opportunity for a further increase of the share of renewables and a reduction of CO_2 emissions. Hydrogen production through electrolysis or generally power-to-gas technologies can be used both as a negative power reserve and as a power arbitrage method [1].

Nevertheless, modern gas turbines face several problems when operating on hydrogen-enriched fuels including flashback, combustion instabilities, and increased emissions. Furthermore, there are several considerations about the changes in the compressor-turbine matching and the cooling of the first turbine stages [2]. As gas turbines are major gas consumers, these issues are important restrictions of the upper limit of hydrogen concentration in the existing natural gas network.

There is an extensive body of research on premixed flames of hydrogen-enriched fuels on both industrial [3–5] and generic combustion systems, mostly focusing on flame stability, emissions and flashback. Hydrogen addition evidently lowers the LBO limit of swirl-stabilized combustors irrespective of the combustion system details, even for relatively low hydrogen concentrations in the fuel. Schefer

*Address all correspondence to this author at stathopoulos@tu-berlin.de.

et al. [6] came to this conclusion by studying the effects of hydrogen enrichment in methane–air mixtures on a generic combustor with a center body and a swirled annular premixed fuel–air jet. The stabilizing effect of hydrogen enrichment has been also confirmed in the results of Mayer *et al.* [7] for the case of a swirl-stabilized combustor without a center body. Equivalent results were also presented by Griebel *et al.* [8], who carried out experiments in a generic, high-pressure combustor with a sudden expansion geometry for flame stabilization. Zhang *et al.* [9], on the other hand, concentrated on the blowout dynamics of hydrogen-enriched flames in a combustion system comparable to that in [6]. Zhang *et al.* pointed out that relatively low hydrogen enrichment has no impact on the blowout phenomena, whereas for higher enrichment extinction/re-ignition phenomena lead to highly dynamic blowout sequences. The observed dynamic blowout phenomena were demonstrated as complex interference between the vortex breakdown zones and blowout and re-ignition phenomena [9].

In contrast to the effect of hydrogen enrichment on LBO, researchers came to different conclusions about its effect on emissions. In fact, Schefer *et al.* [6] claimed that hydrogen enrichment had no impact on NO_x emissions as long as the flame temperature was kept constant, whereas CO emissions were reduced with enrichment. By contrast, several researchers [8, 10] claimed that hydrogen enrichment had no measurable effect on CO emissions. They reported however that an increase of NO_x emissions was observed and they attributed this effect to the chemical influence of hydrogen enrichment on the NO_x formation processes. An increase of NO_x emissions due to hydrogen enrichment of natural gas has also been reported in commercial swirl-stabilized combustion systems and it was attributed to the same cause [5, 11].

The challenges introduced in the design of swirl-stabilized combustion systems by hydrogen addition have also been the focus of several researchers. In particular, Kim *et al.* [12] focused on the effect of swirl on flame shape and emissions, while they analyzed primarily the effects in the main flame zone. Sangl *et al.* [13] and Mayer *et al.* [7], on the other hand, presented a way to actively influence the flow field of a swirl-stabilized combustion system so that it can be adapted to various reactivities of the fuel mixture. They sought to achieve this goal by introducing axial air and fuel injection to change the position of the inner recirculation zone in the combustion chamber and increase the flashback resistance of the system.

The combustion system of the current work also uses axial air and fuel injection to control the position of the vortex breakdown zone. A thorough presentation of the system design, its stability maps and the respective emissions in experiments with pure hydrogen at atmospheric pressure have been presented in the works of Reichel *et al.* [14, 15]. Kuhn *et al.* [16] extended this work by performing experiments in a very wide range of conditions, ranging from pure hydrogen to steam diluted natural gas. The current work aims to extend the results of Kuhn *et al.* [16] and present the performance of the combustion system at higher pressures.

In the following sections, the experimental facility used for the high-pressure experiments is briefly described along with the combustion system and the measurement procedure. The emissions of the system are then presented and the work is concluded with the analysis of the results of a reaction network model.

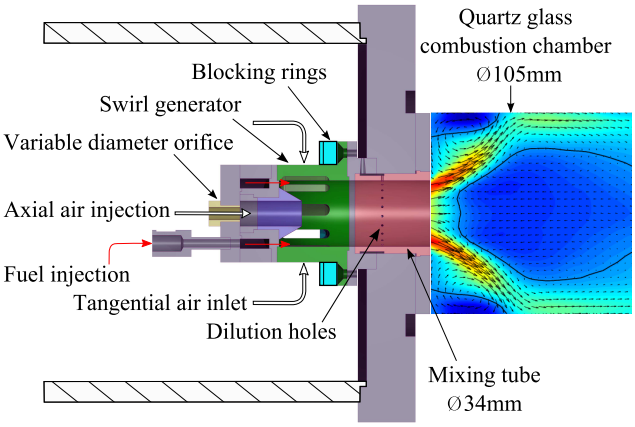

Fig. 1. COMBUSTION SYSTEM AS USED IN THE ATMOSPHERIC EXPERIMENTS

EXPERIMENTAL SETUP AND OPERATING CONDITIONS

Swirl-stabilized combustor

A sketch of the combustor is presented in Fig. 1. It consists of a radial swirl generator followed by a mixing tube and a cylindrical combustion chamber. Air enters the mixing tube through the ports of the radial swirl generator (green) and an orifice in the main axis of the combustor (yellow). The flow swirl number can be adjusted by changing the surface area of the swirl generator ports with the help of blocking rings. The proportion of the total air flow that is directed to the axial injection is not directly controlled. Instead, the pressure drop of the two passages, swirl generator and central orifice, is adjusted by changing their surface area. This air proportion was kept constant throughout the experiments presented in the current work, and it was determined from previous velocity field measurements [15]. Fuel is injected into the mixing tube through 16 injection holes located around the axial air injection orifice. The mixing tube is designed to provide enough residence time to the reactants for good fuel–air mixing. In the work of Reichel *et al.* [14], the fuel–air mixing quality was studied for the current combustor setup and other configurations by means of laser-induced fluorescence. Within this study [14], the current setup showed very good spatial and temporal mixing quality, having a spatial unmixedness factor of $U_s = 2.37 \cdot 10^{-4}$ and a temporal unmixedness factor of $U_t = 4.2 \cdot 10^{-4}$. Moreover, no further decrease in NO_x emissions was found for temporal and spatial

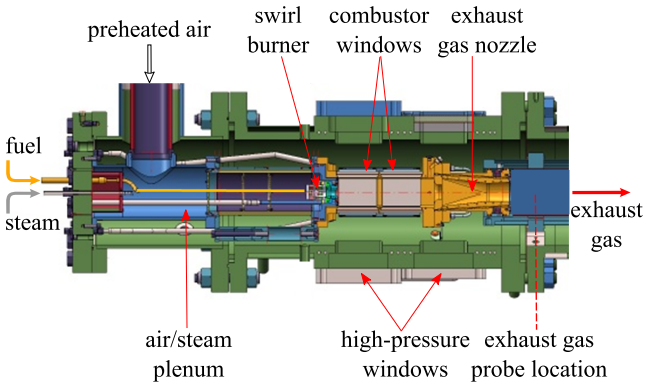

Fig. 2. COMBUSTOR WITH OPTICAL ACCESS INTEGRATED IN THE HBK-S

unmixedness factors below 10^{-3}. Flashback in the boundary layer of the mixing tube is avoided by diluting the mixture with air near the walls. This is achieved by drilling air dilution holes in the circumference of the mixing tube and choosing the residence time of the reactants below their autoignition delay times [14].

High pressure test rig

Table 1. NATURAL GAS COMPOSITION

Component	Concentration (vol.%)
Methane	90.7-96.3
Ethane	3.8-4.8
Propane	0.4-0.7
Nitrogen	1.4-2.8
Carbon Dioxide	1.1-1.5

The measurements at elevated pressures were carried out in the high-pressure combustor rig (HBK-S) at the DLR Stuttgart. In this optically accessible rig, geometrically scaled combustors can be investigated with optical diagnostics at gas turbine relevant operating conditions. The air supply system (main, cooling, secondary air) is capable of delivering a total mass flow of 1.3 kg/s at a maximum pressure of 40 bar. The main air can be electrically preheated up to 1000 K, while experiments with various gaseous and liquid fuels are possible. In this study, natural gas (NG) and a NG/hydrogen blend of 90/10% by mass were used. The natural gas composition used in the experiments is presented in Tab. 1 and a more detailed description of the HBK-S can be found in [17]. A light fuel oil fired steam generator was used to generate saturated steam up to a mass flow rate of 250 g/s. The mass flow rates of air, steam, natural gas and hydrogen were measured with Coriolis flow meters with an accuracy in the order of $\pm 1\%$.

Figure 2 shows the optically accessible combustion chamber integrated in the HBK-S. Steam was guided in an insulated stainless-steel pipe to the supply flange of the high-pressure casing. Preheated main air and steam were mixed in the air/steam plenum and subsequently fed to the swirl combustor. A K-type thermocouple placed at the exit of the air/steam plenum measured the combustor inlet temperature, which was in turn controlled with an accuracy of ± 2K. The fuel mixture of the experiments with hydrogen-enriched natural gas was prepared outside the pressure casing. A K-type thermocouple, positioned in the fuel plenum of the combustor, was used to measure the fuel temperature and was found to be in the range between 326 and 545 K. An example of the fuel injection temperatures is presented in Fig. 3. As the fuel stream was not preheated, the differences in the fuel temperature at the inlet of the combustion system are a result of heat transfer from the air plenum to the fuel stream. The respective heat transfer coefficients depend strongly on the fuel composition and flow rate, which consequently resulted in a different fuel injection temperature for each operational condition of the combustion system.

The combustion chamber has a rectangular cross-section of 100 mm$\times$140 mm and is 280 mm long. The exhaust gases were led out of the combustion chamber through a water-cooled exhaust gas nozzle with a length of 305 mm, a minimal inner diameter of 50 mm and a sudden expansion (see Fig. 2). In addition, this geometry resulted in total residence times in the range of 20-35 ms, based on the operating conditions reported in the present work.

About 5% of the main air flow rate was used for the impingement-cooling of the combustor front panel. The cooling air entered the combustor through small slots close to the liner walls. A sandwich of an inner and an outer quartz glass window is embedded in a water-cooled metal frame, forming the liner. Similarly, convective cooling with a separately controlled air stream was applied at the windows. Several sensors monitored and recorded the experimental conditions and the temperature of the combustor wall to prevent

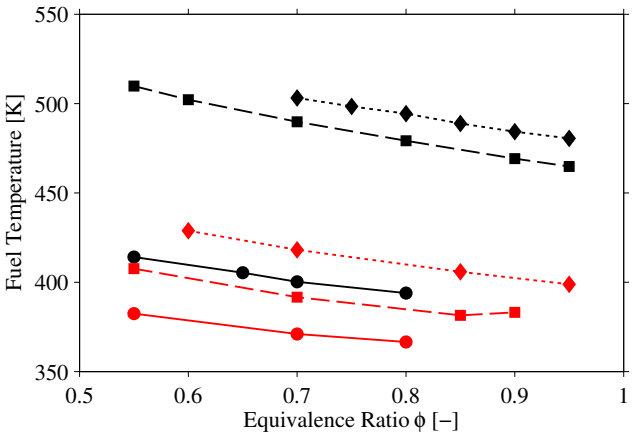

Fig. 3. FUEL TEMPERATURE FOR 100% NG ● AT $p = 4$ bar AND THE MIXTURE OF 90% NG AND 10% BY MASS HYDROGEN ● AT $p = 5$ bar AND STEAM CONTENTS (● — $\Omega = 0$ / ■ - - $\Omega = 0.1$ / ◆··· $\Omega = 0.2$/($\Omega = 0.25$ FOR THE MIX))

overheating of the combustor front panel.

The flow rates and the inlet and outlet temperatures of the cooling flows were measured in order to calculate the convective heat losses at the air-cooled windows, water-cooled metal frame, and the air-cooled exhaust gas nozzle. These measurements were used in the reactor network models to estimate the overall heat loss of the network. As expected, the relative total heat loss decreased with pressure and was in the range of 4-11% for the combustion chamber and 12-22% for the exhaust gas nozzle.

The major gas species and the NO_x and CO emissions were measured with a gas probe located 80 mm downstream of the exhaust gas nozzle, using an exhaust gas analysis system at dry conditions. The uncertainty of the emission measurements is typically better than $\pm 3\%$, including the measuring error of the exhaust gas analyzers (typically $\pm 1\%$) and the uncertainty of the O_2 measurements. A flame ionization detector was used to monitor unburned hydrocarbons (UHC) emissions at wet conditions but no UHC emissions were observed during the measurements.

Operating conditions

The steam-to-air mass flow ratio used in the current work is defined by Eqn. (1), where $\dot{m}_{steam}$ and $\dot{m}_{air}$ are the mass flow rates of steam and main air, respectively.

$$\Omega = \frac{\dot{m}_{steam}}{\dot{m}_{air}} \tag{1}$$

Table 2 presents the operating conditions during the experiments presented in the current work. The mass flow rates of air and steam were kept constant for all measurements at a given pressure level. At 1 bar their sum was 50 g/s, increasing to 300 g/s at 9 bar. For a typical measurement series, the equivalence ratio was increased in steps starting from $\phi = 0.5$ until either flashback occurred or the value of $\phi = 0.95$ was reached.

Table 2. OPERATING CONDITIONS

Parameter	Value
Combustor air inlet temperature (K)	673
Pressure (bar)	4, 5, 9
Steam content, Ω (%)	0, 10, 20, 25
Thermal power (kW)	between 70 and 800

EXPERIMENTAL RESULTS

Flame position and shape

The influence of pressure and steam injection on the flame shape and position is displayed in Fig. 4 for the natural gas flame and in Fig. 5 for the mixture of natural gas and hydrogen. Each OH*-chemiluminescence image is normalized by the respective maximum intensity value. In both figures pressure is increased from left to right and the steam-to-air mass ratio Ω increases from top to bottom. The first column corresponds to the atmospheric tests, conducted in a cylindrical quartz glass combustion chamber with diameter 105 mm, while the high pressure flames are situated in a rectangular (100 mm$\times$140 mm) combustion chamber. Despite the differences in the combustion chamber geometries, both atmospheric and high pressure conditions lead to comparable results in terms of flame shape and position. The flame position, depicted by the white stars, is estimated by the center of mass of the flame region with an intensity of more than 70% of the maximum intensity at each case. For the highest steam content the atmospheric natural gas flame was slightly unstable, resulting in a blurry average intensity distribution. The presented images were recorded at a constant equivalence ratio of $\phi = 0.8$ for the natural gas measurements and $\phi = 0.85$ for the hydrogen-enriched fuel mixture, for all pressure and steam levels. For the case with pure natural gas presented in Fig. 4, the flame shape remained relatively constant for all three pressure levels, except for the atmospheric case at highest steam content.

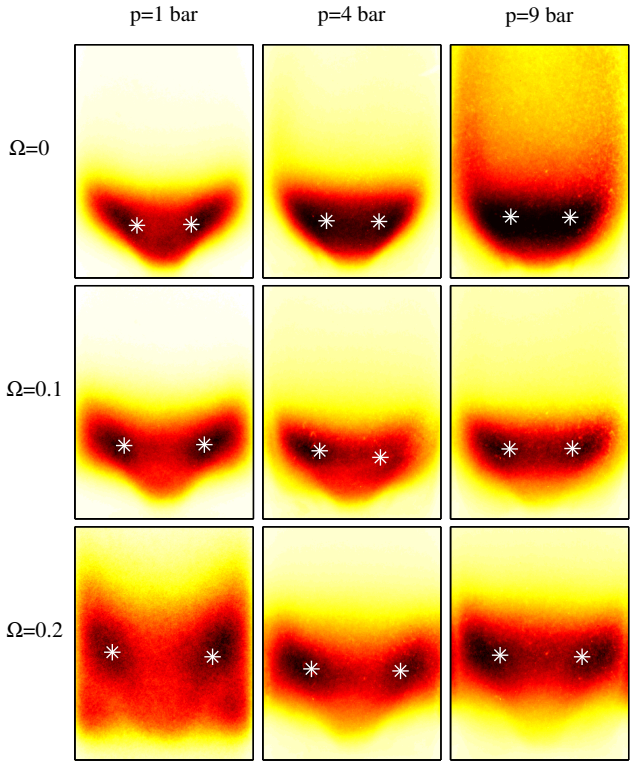

Fig. 4. NORMALIZED OH*-CHEMILUMINESCENCE IMAGES FOR 100% NATURAL GAS AT CONSTANT EQUIVALENCE RATIO OF $\phi = 0.8$

The influence of steam dilution, pressure, and fuel composition on the flame position and shape is presented in Fig. 6 and 7, in which the axial and radial flame positions are shown for the tested experimental conditions. Concentrating on the axial position of dry flames ($\Omega = 0$), it can be observed that

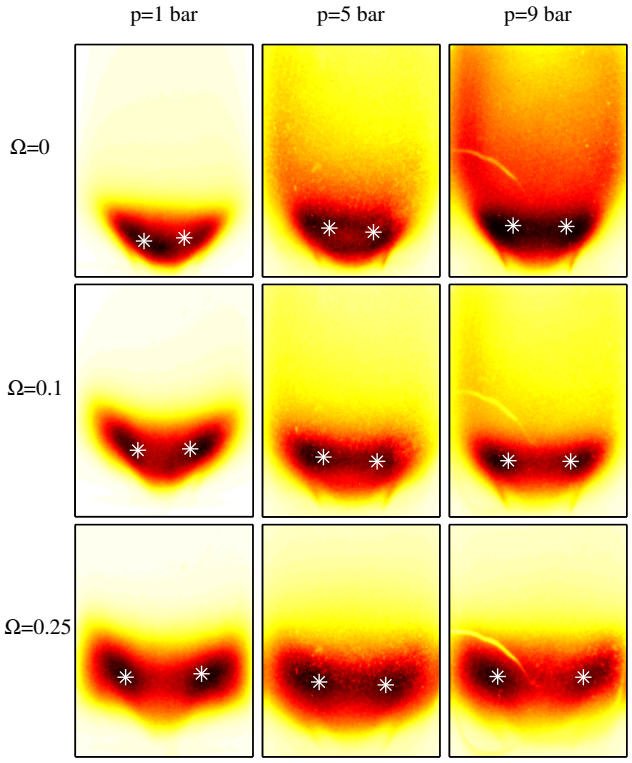

Fig. 5. NORMALIZED OH*-CHEMILUMINESCENCE IMAGES FOR 90% NATURAL GAS AND 10% HYDROGEN BY MASS AT CONSTANT EQUIVALENCE RATIO OF $\phi = 0.85$. Left column from [16]. (THE TOP RIGHT IMAGE (9 bar, $\Omega = 0$) REPRESENTS A 95% NATURAL GAS AND 5% HYDROGEN BY MASS FLAME)

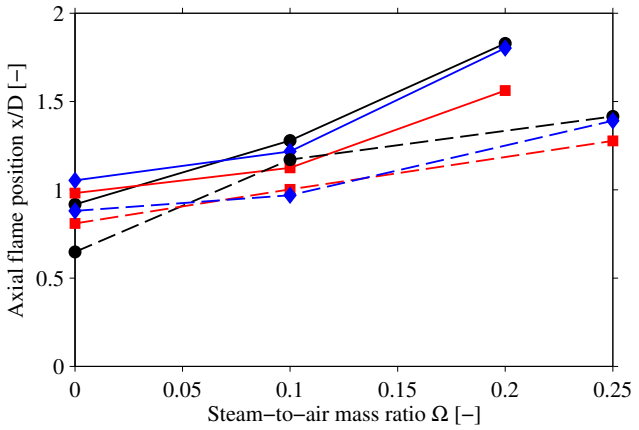

Fig. 6. AXIAL FLAME POSITION AS A FUNCTION OF STEAM DILUTION AND PRESSURE FOR BOTH FUEL MIXTURES. NATURAL GAS (● — $p = 1$ bar / ■ — $p = 4$ bar / ◆ — $p = 9$ bar) AND FUEL MIXTURE (● - - $p = 1$ bar / ■ - - $p = 5$ bar / ◆ - - $p = 9$ bar)

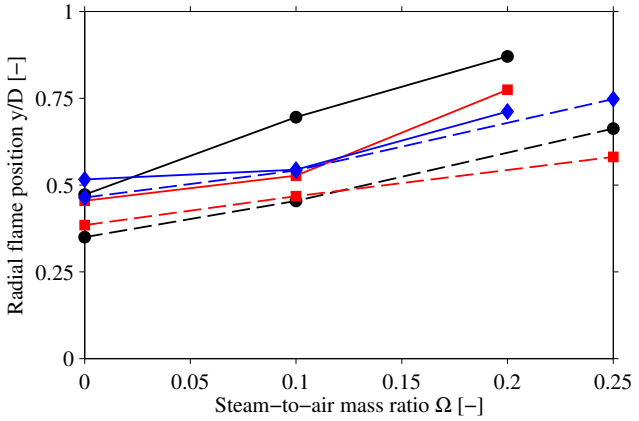

Fig. 7. RADIAL FLAME POSITION AS A FUNCTION OF STEAM DILUTION AND PRESSURE FOR BOTH MIXTURES. NATURAL GAS (● — $p = 1$ bar / ■ — $p = 4$ bar / ◆ — $p = 9$ bar) AND FUEL MIXTURE (● - - $p = 1$ bar / ■ - - $p = 5$ bar / ◆ - - $p = 9$ bar)

an increase in pressure shifted the flame downstream for both investigated fuel compositions. On the other hand, the addition of hydrogen in the fuel mixture had the opposite effect and the flame was shifted upstream closer to the burner outlet. Figure 6 also reveals that increasing steam dilution continuously shifted the axial flame position downstream irrespective of the fuel mixture used. Concerning the radial flame position, which gives an indication of how compact a flame is, Fig. 7 shows that steam dilution shifted the radial flame position outwards, thus, making it less compact. The addition of hydrogen had exactly the opposite effect for all investigated pressures, making the flame more compact. Interestingly, increasing pressure seemed to have no practical effect on the compactness of natural gas flames, whereas the data indicates that the hydrogen-enriched natural gas flame became less compact at elevated pressure levels.

The presented flame is stabilized at two V-shaped shear layers produced by the typical vortex breakdown flow field. As a result, changes in burning velocity lead to a downstream or upstream propagation of the flame front. The experimental and numerical study of Göckeler [18] showed that the dilution with steam strongly reduces the laminar flame velocity for methane as well as for hydrogen-enriched methane flames. This observation can be attributed to the reduction of the reactive species concentration and the increased heat capacity of the mixtures as well as to a direct chemical effect. Furthermore, Albin *et al.* [19] showed that the decrease in burning velocity due to steam dilution was similar for laminar and turbulent methane flames. These observations explain the slight downstream shift of the flame and its spatially less confined structure as a result of an increase in steam content. The same trends are also observed in Fig. 5 for the mixture of natural gas and hydrogen.

More generally, Göckeler *et al.* [20] have shown that the burning velocity exhibits a maximum for a certain equivalence ratio and increases with higher hydrogen fuel content. In particular, for natural gas–hydrogen mixtures, with relatively high natural gas concentration, the burning velocity increases quasi-linearly with the hydrogen content as reported by Boushaki *et al.* [21]. In this case, the influence of the large mass fraction of hydrogen is much higher than the small variation of the equivalence ratio. This increase in burning velocity made the hydrogen-enriched flame more compact and lead to its centralization near the stagnation point for the

dry case. With increasing steam dilution the flame widened again.

NO_x emissions

The formation of NO_x emissions strongly depends on pressure and it is known to increase exponentially with the flame temperature [8, 10, 18]. Figures 8 and 9 present the measured NO_x emissions. The black lines represent data of the atmospheric measurements conducted in the cylindrical combustion chamber, whereas the emissions at elevated pressure were measured in the high pressure test rig. As a result, the scaling of NO_x emissions is considered to be a rather qualitative and not an absolute trend. Although the differences in the combustion chamber geometry and experimental setups between the atmospheric [16] and high-pressure tests are not insignificant, the measured NO_x emissions reflect the substantial increase with pressure. This increase can be expressed by the exponential scaling law presented in [22]

$$\text{Emissions}\,(p) = \text{Emissions}\,(p_0)\left(\frac{p}{p_0}\right)^{\alpha}, \qquad (2)$$

with p_0 being a reference pressure and α, the scaling exponent. This scaling law was shown to be applicable at steam diluted conditions [23].

The increase of NO_x with pressure markedly affected the cases without steam injection ($\Omega = 0$), resulting in high emissions even at low adiabatic flame temperatures. This effect was even more pronounced for the hydrogen-enriched fuel. In this case, the exponent α is approximately 0.55, compared to 0.4 for the natural gas experiments. Those exponents are obtained by scaling the NOx emissions from intermediate pressure (5 bar and 4 bar respectively) to high pressure (9 bar). Scaling emissions from 1 bar to higher pressure levels consistently results in higher exponents α in the range of 0.6 to 0.9 for both fuel compositions and at various steam injection rates. This finding reflects the differences in combustion chamber geometry and cooling. With a steam injection rate of 10%, the NO_x formation was considerably reduced for both fuel compositions. At elevated pressures, however, an injection rate of 10% was not sufficient to achieve low NO_x emissions in the entire operational range, especially in the case of hydrogen enrichment ($\alpha = 0.7$ compared to 0.5 for 100% NG). At the highest tested rates of steam dilution, a substantial reduction of NO_x was achieved for both fuel compositions up to the highest investigated pressure and equivalence ratio. Here, the scaling law could not be applied due to consistently low NO_x emissions (< 10 ppm for 100% NG and < 5 ppm for the hydrogen-enriched NG), which were in the order of magnitude of the described measurement uncertainties.

CO emissions

The measured CO emissions are presented in Fig. 10 and 11. As for the NO_x emissions, the black lines represent data at 1 bar, obtained in the atmospheric test rig. When plotted with respect to the equivalence ratio, the CO emissions

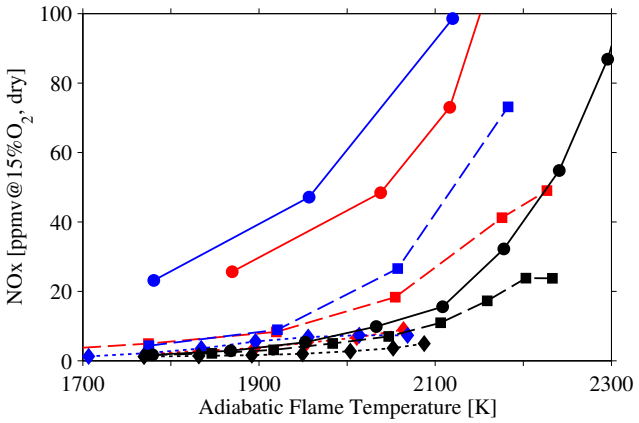

Fig. 8. NO_x EMISSIONS FOR 100% NATURAL GAS AT VARIOUS PRESSURE LEVELS (● — $p = 1$ bar / ● — $p = 4$ bar / ● — $p = 9$ bar) AND STEAM CONTENTS (● — $\Omega = 0$ / ■ - - $\Omega = 0.1$ / ◆ ··· $\Omega = 0.2$)

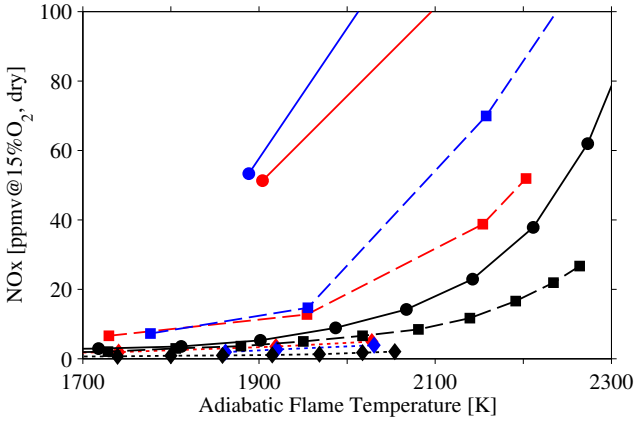

Fig. 9. NO_x EMISSIONS FOR 90% NATURAL GAS AND 10% HYDROGEN BY MASS AT VARIOUS PRESSURE LEVELS (BY $\Omega = 0$ AND $p = 9$ bar 95% NATURAL GAS AND 5% HYDROGEN BY MASS) (● — $p = 1$ bar / ● — $p = 5$ bar / ● — $p = 9$ bar) AND STEAM CONTENTS (● — $\Omega = 0$ / ■ - - $\Omega = 0.1$ / ◆ ··· $\Omega = 0.25$)

seem to be reduced by the injection of steam. However, in order to achieve the same adiabatic flame temperature with steam injection, higher equivalence ratios were required due to the cooling effect of steam. Consequently, when the emissions are compared at the same adiabatic flame temperature, a slight increase of CO with increasing steam content can be observed.

In the present study, the influence of pressure on CO emissions was not as distinct as for the NO_x emissions. Generally, CO decreases at elevated pressure [24, 25], and is known to follow the scaling law in Eqn. (2) with α in the range of -0.4 to -0.5. Since the CO emissions at 1 bar were obtained in the atmospheric test rig, the scaling law can only be applied to the data at elevated pressure, due to the sensitivity of CO formation on the experimental setup [6]. This circumstance is reflected by a lower exponent α in the or-

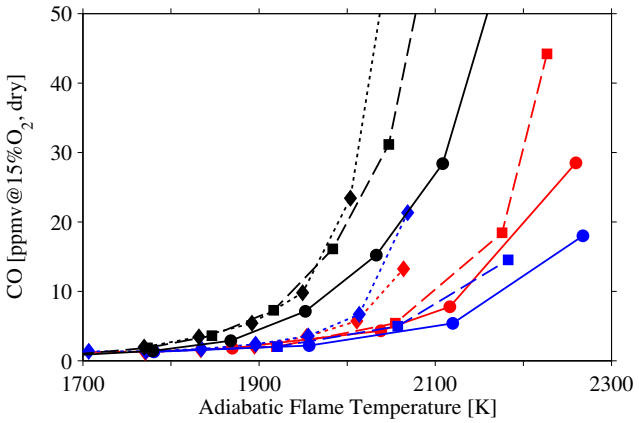

Fig. 10. CO EMISSIONS FOR 100% NATURAL GAS AT VARIOUS PRESSURE LEVELS (● — $p = 1$ bar / ● — $p = 4$ bar / ● — $p = 9$ bar) AND STEAM CONTENTS (● — $\Omega = 0$ / ■ - - $\Omega = 0.1$ / ◆ ··· $\Omega = 0.2$)

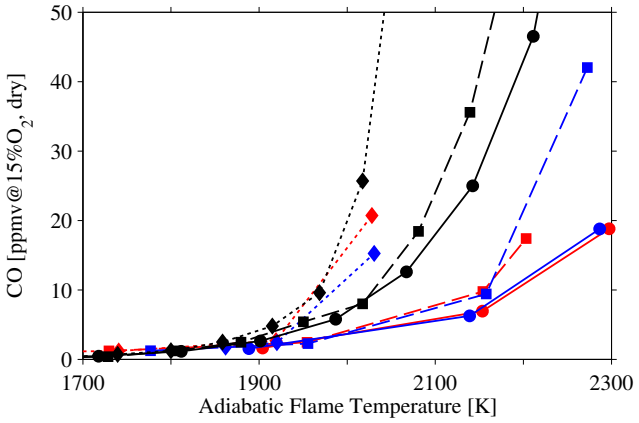

Fig. 11. CO EMISSIONS FOR 90% NATURAL GAS AND 10% HYDROGEN BY MASS AT VARIOUS PRESSURE LEVELS (BY $\Omega = 0$ AND $p = 9$ bar 95% NATURAL GAS AND 5% HYDROGEN BY MASS)(● — $p = 1$ bar / ● — $p = 5$ bar / ● — $p = 9$ bar) AND STEAM CONTENTS (● — $\Omega = 0$ / ■ - - $\Omega = 0.1$ / ◆ ··· $\Omega = 0.25$)

der of -0.8 when back-scaling the measured CO emissions from 4 bar (Ω=0, 100% natural gas) to the atmospheric measurements at the same conditions. In Fig. 10 a decrease of CO at dry conditions is observed from 4 bar to 9 bar, following Eqn. (2) with α=-0.5. The decrease of CO emissions at steam diluted conditions however, was not consistent with the aforementioned scaling law, in the specific case from intermediate to the highest pressure level. Nevertheless, CO was significantly reduced compared to atmospheric conditions. For the mixture of natural gas and hydrogen (Fig. 11), CO emissions were relatively low at elevated pressure levels. Except for higher adiabatic flame temperatures, the lines of CO at 5 bar and 9 bar collapsed. Although no quantitative trend can be determined based on the current study, steam injection shows excellent results at elevated pressure levels. Especially for the hydrogen-enriched fuel composition, it is considered beneficial, not only in terms of NO_x reduction, but also due to low CO formation and an enhanced operational range.

REACTOR NETWORK MODELLING

A chemical reactor network implemented in Cantera [26] is employed to analyze the reaction kinetics and pollutant emission formation in the combustor. It has been shown by previous authors [27, 28] that the flame of a well-premixed, swirl-stabilized combustor can be modeled by a combination of a single perfectly stirred reactor (PSR) for the flame followed by a plug flow reactor (PFR) for the post flame zone (PFZ). This approach has been successfully applied by Göke *et al.* [23] and is also used in the current study, as mixing experiments showed that the mixing quality of the gases in the mixing tube of the combustion system is sufficiently good [16]. All gases inside a PSR are perfectly and instantaneously mixed resulting in a uniform composition and temperature within the reactor. In a PFR, temperature and composition vary along the reactor, i.e., in the flow direction, but not in its cross section. In Cantera, a PFR is modeled by interconnected PSRs in series.

The applied network model consists of 26 perfectly stirred reactors (PSR) in series (see network schematic in Fig. 12). A further refinement with more PSRs does not lead to significantly different results in the PFZ [29]. The air, fuel and steam mass flows are injected into the flame reactor where the combustion of the mixture is initiated. In the following 25 reactors, the oxidation of the fuel proceeds through a complex scheme of coupled reaction chains. A detailed reaction mechanism models the participating species and the elementary chemical reactions and reaction rates leading to the final combustion products. An optimized methane-air mechanism, the GRI-Mech 3.0 [30, 31], is applied for the network calculations. It consists of 53 species and 325 elementary reactions including NO_x formation.

In the flame reactor and the first five reactors of the PFZ, the flame heat loss due to radiation from CO_2 and H_2O molecules is taken into account with the help of a gray gas radiation model [32, 33]. During the tests, the temperatures of the cooling air and water were measured at the combustion chamber inlet and outlet and at the exhaust nozzle for all tested operating conditions. The temperature data is used to estimate the overall convective heat loss of the setup, which is distributed homogeneously over the network. The resulting amounts of heat loss are included in the reactors' energy equations. The reactor volumes are estimated from the OH*

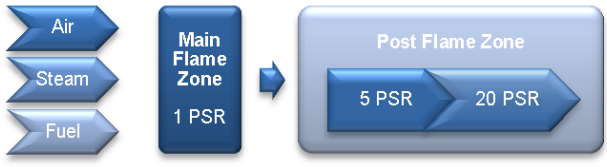

Fig. 12. SCHEMATIC OF THE REACTOR NETWORK MODEL

measurements and the dimensions of the experimental setup.

Simulation results and discussion

The aim of the reactor network simulations is to study the influence of pressure, steam injection and hydrogen enrichment on NO_x generation. To that end, the simulations modeled the experiments with natural gas and a mixture of natural gas and hydrogen with 10% mass fraction of hydrogen in the fuel. The range of equivalence ratio and adiabatic temperature values tested during the experiments and simulated here varied from lean to near stoichiometric conditions and from approximately 1600°C to 2200°C. The simulations considered the pressures $p = [1, 4/5, 9]$ bar and the steam diluted experiments with steam-to-air mass ratios $\Omega = [0.0, 0.1, 0.25]$ were taken into account.

Figure 13 presents the results of the simulations for both mixtures, which are generally in good agreement with the measurements. The individual deviations between simulation results and experimental values can be attributed to two effects. On the one hand, the heat transfer model is not able to perfectly reproduce the exact temperature and heat transfer conditions in the combustion chamber, which in addition are only known to a limited extent. On the other hand, the chemical reaction mechanisms used and the reference emissions measurements are always connected with a certain uncertainty. Nevertheless, the effects of the changes in the adiabatic flame temperature, steam dilution, pressure and fuel composition on the emissions are well captured by the reactor network model.

Four main pathways contribute to the formation of nitric oxides: the thermal (or Zeldovich), the prompt (or Fenimore), the NNH and the N_2O pathway. In the chemical reactor network, the contribution of each pathway to the overall NO_x emissions can be investigated by disabling the pathway specific reaction equations in the applied reaction mechanism. The NO_x formation stemming from the eliminated pathway can be extracted by comparison with the results from the original reaction mechanism. This approach is justified as the emissions calculated for the individual pathways add up to >95% of the original level received with the unchanged mechanism including all pathways at once [18].

In the present study, a formation pathway analysis was carried out for the hydrogen-enriched natural gas fuel at 1 and 9 bar and its results are presented in Fig. 14. As it can be seen, the increase of NO_x emissions with pressure for both dry mixtures is caused mainly by the increase of the NO_x produced through the thermal pathway, even when the emissions are compared at the same equivalent flame reactor temperature. In the dry cases an increase in pressure had a minor impact on the other pathways. It slightly reduced the influence of the prompt and the NNH pathways. If the equivalence ratio is held constant, the thermal effect of steam injection consists of a reduced average flame temperature compared to the dry case. Therefore, a direct analysis of the effect of increased pressure on the steam diluted flame is not possible with the available data set. Yet, the influence of steam injection at constant pressure can be observed. It was

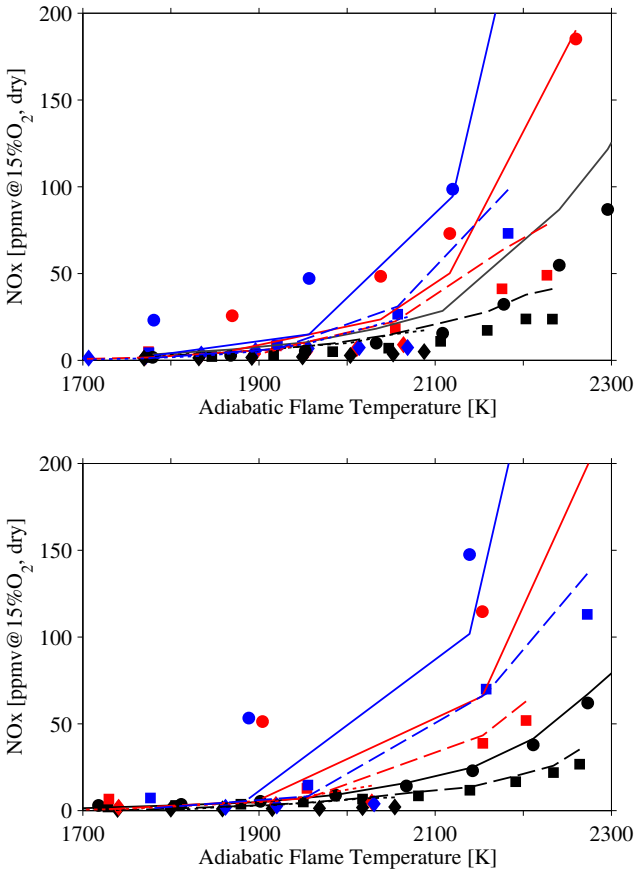

Fig. 13. MEASURED AND SIMULATED NO_x EMISSIONS FOR NATURAL GAS (TOP) AND H_2-ENRICHED NATURAL GAS (BOTTOM) FOR VARIOUS PRESSURES (● — $p = 1$ bar / ● — $p = 4$ bar (TOP), $p = 5$ bar (BOTTOM) / ● — $p = 9$ bar) AND STEAM CONTENTS (● — $\Omega = 0$ / ■ - - $\Omega = 0.1$ / ◆ ··· $\Omega = 0.2$ (TOP), $\Omega = 0.25$ (BOTTOM))

found that steam injection leads to a reduction of NO_x emissions because it suppresses the thermal and N_2O pathways. In addition to the described dilution and thermal effects, the influence of steam also stems from a significant reduction of the oxygen radical concentration in the flame as indicated by Göckeler [18].

CONCLUSIONS

The presented experimental results focused on the influence of pressure, steam dilution and hydrogen enrichment on the emissions and the flame shapes produced from a generic swirl-stabilized combustion system.

The increase of flame burning velocities with pressure and hydrogen enrichment was shown to slightly change the shape and position of the flame. In accordance with literature, increased combustion pressure causes a rise in NO_x emissions, mainly due to an enhancement of the thermal pathway. Steam injection has been proven beneficial for NO_x reduction especially at higher pressure levels, without detrimentally affecting CO emissions. In the particular case of

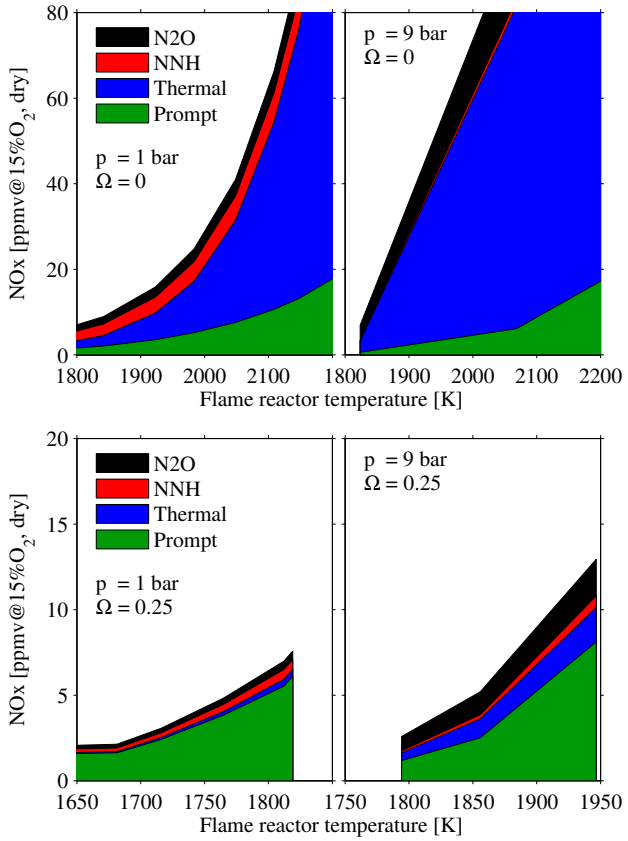

Fig. 14. CONTRIBUTIONS OF THE NO_x FORMATION PATHWAYS IN THE H_2-ENRICHED NATURAL GAS FLAME AT 1 bar (LEFT) AND 9 bar (RIGHT) WITH STEAM CONTENTS $\Omega = 0$ (TOP) AND $\Omega = 0.25$ (BOTTOM)

hydrogen-enriched mixtures and high combustion pressures, it was shown that relatively high steam injection levels are necessary to keep the NO_x emissions at levels acceptable in gas turbine applications. Nevertheless, these levels still lie at the region of the thermodynamic optimum steam injection for most commercial gas turbine applications [34].

Acknowledgements

The research leading to these results has received funding from the European Research Council under the ERC grant agreement: 247322, GREENEST. The authors would like to thank Andy Göhrs for his support in the lab and helpful discussions. The authors would also like to thank R. Schieferstein, S. Peukert, and T. Schiek for their technical support during the high-pressure measurements.

References

[1] Melaina, M., Antonia, O., and Penev, M., 2013. *Blending hydrogen into natural gas pipeline networks: a review of key issues*. No. March. National Renewable Energy Laboratory.

[2] Chiesa, P., Lozza, G., and Mazzocchi, L., 2005. "Using Hydrogen as Gas Turbine Fuel". *Journal of Engineering for Gas Turbines and Power,* ***127***(1), p. 73.

[3] Wu, J., Brown, P., Diakunchak, I., Gulati, A., Lenze, M., and Koestlin, B., 2007. "Advanced Gas Turbine Combustion System Development for High Hydrogen Fuels". In Volume 2: Turbo Expo 2007, ASME, pp. 1085–1091.

[4] Bonaldo, A., Mats, A., and Anders, L., 2014. "Engine Testing Using Highly Reactive Fuels on Siemens Industrial Gas Turbines". *Proceedings of ASME Turbo Expo 2014: Turbine Technical Conference and Exposition*, pp. 1–9.

[5] Lam, K.-K., Geipel, P., and Larfeldt, J., 2014. "Hydrogen Enriched Combustion Testing of Siemens Industrial SGT-400 at Atmospheric Conditions". *Journal of Engineering for Gas Turbines and Power,* ***137***(2), Sept., p. 021502.

[6] Schefer, R., Wicksall, D., and Agrawal, A., 2002. "Combustion of hydrogen-enriched methane in a lean premixed swirl-stabilized burner". *Proceedings of the Combustion Institute,* ***29***(1), Jan., pp. 843–851.

[7] Mayer, C., Sangl, J., Sattelmayer, T., Lachaux, T., and Bernero, S., 2012. "Study on the Operational Window of a Swirl Stabilized Syngas Burner Under Atmospheric and High Pressure Conditions". *Journal of Engineering for Gas Turbines and Power,* ***134***(3), p. 031506.

[8] Griebel, P., Boschek, E., and Jansohn, P., 2007. "Lean Blowout Limits and NOx Emissions of Turbulent, Lean Premixed, Hydrogen-Enriched Methane/Air Flames at High Pressure". *Journal of Engineering for Gas Turbines and Power,* ***129***(2), p. 404.

[9] Zhang, Q., 2007. "Impacts of hydrogen addition on near-lean blowout dynamics in a swirling combustor". *ASME Turbo Expo 2007: Power for Land, Sea and Air*, pp. 1–10.

[10] Beerer, D., McDonell, V., Therkelsen, P., and Cheng, R. K., 2012. "Flashback, Blow Out, Emissions, and Turbulent Displacement Flame Speed Measurements in a Hydrogen and Methane Fired Low-Swirl Injector at Elevated Pressures and Temperatures". In ASME Turbo Expo 2012: Turbine Technical Conference and Exposition, ASME, pp. 113 – 124.

[11] Lantz, A., Collin, R., Aldén, M., Lindholm, A., Larfeldt, J., and Lörstad, D., 2014. "Investigation of Hydrogen Enriched Natural Gas Flames in a SGT-700/800 Burner Using OH PLIF and Chemiluminescence Imaging". In Proceedings of ASME Turbo Expo 2014: Turbine Technical Conference and Exposition, ASME.

[12] Kim, H., Arghode, V., and Gupta, A., 2009. "Flame characteristics of hydrogen-enriched methane–air premixed swirling flames". *International Journal of Hydrogen Energy,* ***34***(2), Jan., pp. 1063–1073.

[13] Sangl, J., Mayer, C., and Sattelmayer, T., 2011. "Dynamic Adaptation of Aerodynamic Flame Stabilization of a Premix Swirl Burner to Fuel Reactivity Using Fuel Momentum". *Journal of Engineering for Gas Turbines and Power,* ***133***(7), p. 071501.

[14] Reichel, T. G., Terhaar, S., and Paschereit, O., 2014. "Increasing Flashback Resistance in Lean Premixed Swirl-Stabilized Hydrogen Combustion by Axial Air Injection". *Journal of Engineering for Gas Turbines and Power,* ***137***(7), Dec., p. 071503.

[15] Reichel, T. G., Goeckeler, K., and Paschereit, O., 2015. "Investigation of Lean Premixed Swirl-Stabilized Hydrogen Burner With Axial Air Injection Using OH-PLIF Imaging". *Journal of Engineering for Gas Turbines and Power,* ***137***(11), Sept., p. 111513.

[16] Kuhn, P., Terhaar, S., Reichel, T., and Paschereit, C. O., 2015. "Design and Assessment of a Fuel-Flexible Low Emission Combustor for Dry and Steam-Diluted Conditions". In ASME Turbo Expo 2015: Turbine Technical Conference and Exposition, ASME.

[17] Fleck, J. M., Griebel, P., Steinberg, A. M., Stöhr, M., Aigner, M., and Ciani, A., 2010. "Experimental Investigation of a Generic, Fuel Flexible Reheat Combustor at Gas Turbine Relevant Operating Conditions". In ASME Turbo Expo 2010: Power for Land, Sea, and Air: Power for Land, Sea and Air, ASME, pp. 583–592.

[18] Göckeler, K., 2015. "Influence of steam dilution and hydrogen enrichment on laminar premixed methane flames". Phd thesis, TU Berlin.

[19] Albin, E., Nawroth, H., Göke, S., D'Angelo, Y., and Paschereit, C. O., 2013. "Experimental investigation of burning velocities of ultra-wet methane-air-steam mixtures". *Fuel Processing Technology,* ***107***, pp. 27 – 35. Selected Papers from the Eleventh International Conference on Combustion and Energy Utilization (11th ICCEU).

[20] Göckeler, K., Krüger, O., and Oliver Paschereit, C., 2014. "Laminar Burning Velocities and Emissions of Hydrogen-Methane-Air-Steam Mixtures". *Journal of Engineering for Gas Turbines and Power,* ***137***(3), Oct., p. 041505.

[21] Boushaki, T., Dhuè, Y., Selle, L., Ferret, B., and Poinsot, T., 2012. "Effects of hydrogen and steam addition on laminar burning velocity of methane-air premixed flame: Experimental and numerical analysis". *International Journal of Hydrogen Energy,* ***37***(11), pp. 9412 – 9422.

[22] Correa, S. M., 1993. "A Review of NOx Formation Under Gas-Turbine Combustion Conditions". *Combustion Science and Technology,* ***87***(1-6), pp. 329–362.

[23] Göke, S., Schimek, S., Terhaar, S., Göckeler, K., Krüger, O., Fleck, J., Griebel, P., and Paschereit, C. O., 2014. "Influence of Pressure and Steam Dilution on NOx and CO Emissions in a Premixed Natural Gas Flame". *Journal of Engineering for Gas Turbines and Power,* ***136***(9), p. 091508.

[24] Bhargava, A., Kendrick, D. W., Colket, M. B., Sowa, W. A., Casleton, K. H., and Maloney, D. J., 2000. "Pressure effect on NOx and CO emissions in industrial gas turbines". In ASME Turbo Expo 2000: Power for Land, Sea, and Air, American Society of Mechanical Engineers, p. V002T02A017.

[25] Lefebvre, A. H., 1983. *Gas turbine combustion*. Hemisphere Publishing Corporation.

[26] Goodwin, D., 2003. An open source, extensible software suite for CVD process simulation. California Institute of Technology, Division of Engineering and Applied Science.

[27] Beer, J., and Lee, K., 1965. "The effect of the residence time distribution on the performance and efficiency of combustors". *10th International Symposium on Combustion, The Combustion Institute*, pp. 1187–1202.

[28] Michaud, M., Westmoreland, P., and Feitelberg, A., 1992. "Chemical mechanisms of NOx formation for gas turbine conditions". *In Symposium (International) on Combustion,* ***24***, pp. 879–887.

[29] Göke, S., Terhaar, S., Schimek, S., Göckeler, K., and Paschereit, C. O., 2011. "Combustion of natural gas, hydrogen and bio-fuels at ultra-wet conditions". *Volume 2: Combustion, Fuels and Emissions, Parts A and B*.

[30] Smith, G. P., Golden, D. M., Frenklach, M., Moriarty, N. W., Eiteneer, B., Goldenberg, M., Bowman, C. T., Hanson, R. K., Song, S., William C. Gardiner, J., Lissianski, V. V., and Qin, Z., 2000. GRI 3.0.

[31] Curran, H. J., 2004. "Detailed chemical kinetic modeling; is there life after gri-mech 3.0?". *Prepr. Pap.-Am. Chem. Soc., Div. Fuel Chem,* ***49***(1), pp. 263–264.

[32] Leckner, B., 1972. "Spectral and total emissivity of water vapor and carbon dioxide". *Combustion and Flame*, pp. 19:33–48.

[33] Ronney, P., 2003. "Gas radiation: emissivities, absorptivities, Planck mean absorption coefficients and net emission from H2O and CO2 radiation according to the Hottel/Leckner model".

[34] Stathopoulos, P., Terhaar, S., and Paschereit, C., 2014. "The Ultra-Wet Cycle for High Efficiency, Low Emission Gas Turbines". In ETN - IGTC - The future of gas turbine technology.